# Dynamic and real-time continuous look-ahead distance for autonomous vehicles: an explicit formulation

Fadel Tarhini, Reine Talj, Moustapha Doumiati

# Dynamic and real-time continuous look-ahead distance for autonomous vehicles: an explicit formulation

Fadel Tarhini [a], Reine Talj [a] and Moustapha Doumiati [b]

[a]Sorbonne université, Université de Technologie de Compiègne, CNRS, Heudiasyc UMR 7253, CS 60 319, 60 203 Compiègne, France; [b]ESEO-IREENA Lab UR 4642 Nantes University, 10 Bd Jeanneteau, 49100 Angers, France.

**ARTICLE HISTORY**
Compiled Tuesday 26th September, 2023

**Abstract**
The advent of autonomous vehicles has brought about significant advancements in transportation technology, promising safer and more efficient means of travel. However, their full integration into society depends on the accuracy of path-tracking realized by a lateral controller. Lateral control is achieved by regulating the steering angle to minimize the lateral error between the vehicle and a target point at a look-ahead distance on the reference path. This paper investigates the look-ahead distance as it is considered a key parameter that impacts vehicle performance, stability, and energy consumption. A qualitative analysis is performed to deduct a set of rules to adapt the look-ahead distance to three parameters: vehicle velocity, road curvature, and road adherence. Then, an original explicit mathematical formulation is developed for the look-ahead distance as a function of the considered parameters. A fuzzy logic decision for the look-ahead distance is further established and compared with the formulated one. Both approaches are implemented on a look-ahead distance-based lateral controller based on the super-twisting sliding mode control. Simulation results carried out in a joint simulation between Simulink/MatLab and SCANeR$^{TM}$ Studio vehicle dynamics simulator demonstrate the effectiveness of the developed model on vehicle performance, stability, computational efficiency, and energy consumption.

**KEYWORDS**
Autonomous vehicle, look-ahead distance, fuzzy logic, super-twisting sliding mode control

## Nomenclature

| | |
|---|---|
| $\beta$ | Vehicle side-slip angle $[rad]$ |
| $\chi_i$ | Intensity of the slope of the transients-state centroid of $k_i$ $(i = 1, 2)$ |
| $\delta_c$ | Vehicle controlled steering angle $[rad]$ |
| $\eta_j$ | Efficiency of the motor $j$ |
| $\gamma_i$ | Intensity of the slope of the transients-state centroid of $f_i$ $(i = 1, 2)$ |
| $\lambda_{adapt}$ | Adapting gain parameter for $f_3$ |
| $\mu$ | Road adherence |
| $\omega_j$ | Rotational velocity of the motor $j$ $[rad/s]$ |
| $\psi$ | Vehicle yaw angle $[rad]$ |

CONTACT Tarhini. Email: fadeltarhini@hotmail.com

| | |
|---|---|
| $\rho$ | Road curvature $[m^{-1}]$ |
| $\underline{\mu}, \overline{\mu}$ | Extremities of the transient state of $f_3$ and $k_1$ |
| $\underline{\rho}, \overline{\rho}$ | Extremities of the transient state of $f_2$ and $k_2$ |
| $\underline{V}, \overline{V}$ | Extremities of the transient state of $f_1$ |
| $\xi_i$ | Shaping parameters for $f_1$ $(i = 1, 2)$ |
| $\zeta_i$ | Shaping parameters for $f_2$ $(i = 1, 2)$ |
| $a_y$ | Vehicle lateral acceleration $[m/s^2]$ |
| $c, \sigma$ | Mean and standard deviation of the Gaussian functions |
| $E$ | Accumulated energy consumption $[J]$ |
| $e_y$ | Lateral error at the vehicle's center of gravity $[m]$ |
| $e_{y,Ls}$ | Lateral error at the look-ahead distance $Ls$ $[m]$ |
| $f_1$ | Look-ahead distance function of the velocity $[m]$ |
| $f_2$ | Look-ahead distance function of road curvature $[m]$ |
| $f_3$ | Look-ahead distance function of road adherence and curvature $[m]$ |
| $g$ | Gravitational acceleration $[m/s^2]$ |
| $j$ | Index for the four in-wheel motors $j = 1, 2, 3, 4$ |
| $k_1, k_2$ | Component functions of $f_3$ |
| $Ls$ | Look-ahead distance $[m]$ |
| $Ls_{add}$ | Additional look-ahead distance in the fuzzy scheme $[m]$ |
| $Ls_{max_\mu}$ | Upper limit for look-ahead distance adapted to adherence $[m]$ |
| $Ls_{max_\rho}$ | Upper limit for look-ahead distance adapted to curvature $[m]$ |
| $Ls_{max_V}$ | Upper limit for look-ahead distance adapted to velocity $[m]$ |
| $Ls_{min_\mu}$ | Lower limit for look-ahead distance adapted to adherence $[m]$ |
| $T_j$ | Torque of the motor $j$ $[N.m]$ |
| $T_m$ | Total torque generated for longitudinal velocity control $[N.m]$ |
| $V_x$ | Vehicle longitudinal velocity $[km/h]$ |
| $V_{x,des}$ | Desired reference profile for longitudinal velocity $[km/h]$ |

## 1. Introduction

Safety, accessibility, and efficiency, the leading advantages that are quintessential to revolutionizing transportation, are directly conferred by Autonomous Vehicles (AVs). Using advanced sensors and developed algorithms, AVs can rapidly detect and react to their surroundings, significantly reducing the number of accidents caused by driver errors. AVs can communicate among themselves and with traffic management systems to avoid collisions and minimize delays, which reduces traffic congestion and optimizes routes.

The control of an AV is the last step of a chain of tasks including perception, localization, decision-making, and route planning [1]. Several control objectives can be achieved through actuators' coordination, for instance, Advanced Driver Assistance Systems (ADAS). These objectives can solicit the overall motion of the vehicle as in path-tracking [2], or be confined to the chassis dynamics such as enhancing lateral stability [3], or a combination of both [4]. A multi-layer coordinated yaw stability control method based on robust sliding Model Predictive Control (MPC) is implemented in [5] for in-wheel vehicles to improve maneuverability and lateral stability. [6] presented a hierarchical integrated adaptive control strategy for lateral dynamics control via coordination of Active Front Steering (AFS) and Direct Yaw Control (DYC). [7] presented a non-linear integrated control strategy based on an MPC that primarily

focuses on maintaining vehicle lateral stability using AFS and differential braking.

The objectives associated with vehicle chassis control, such as stability and maneuverability enhancement, are instantaneous and relatively straightforward. In contrast to lateral control, which necessitates protracted control over a time horizon, which renders the accomplishment of precise path-tracking sophisticated yet indispensable undertaking pursued by AVs. Trajectory following is achieved by regulating the steering angle to track a reference path based on a lateral controller. [8] presented a safety and comfort-guaranteed automatic following of an AV under several road geometry constraints. A robust adaptive inverse controller is employed in [9] to offset the dynamics of the steering system's backlash for the purpose of path-tracking. [10] developed an efficient MPC for lateral control considering path preview to improve the robustness and computational efficiency in high-speed lateral motion control. A force-driven switched MPC path tracking control strategy is proposed in [11] to improve path tracking accuracy and ensure vehicle stability under handling limit conditions.

Lateral control either based on a geometric or non-geometric model-based approach is achieved by minimizing the lateral displacement error between the vehicle and the reference road, at a look-ahead distance in front of the vehicle. Look-ahead distance-based lateral controllers have been heavily researched since the 90s. [12] proposed a method that generates the vehicle steering angle command by combining fuzzy logic with the geometric pure-pursuit (PP) technique, considering four parameters for the look-ahead distance. Using clothoidal constraints, [13] designed an output measurement matrix to consider look-ahead distance in the kinematic vehicle lateral motion model. Based on the PP geometric method, [14] proposed an adaptive Brownian motion salp swarm algorithm to optimize the look-ahead distance. [15] designed a controller that minimizes the steering angle rate by determining a proper look-ahead distance by solving an optimization control problem. Other recent studies depended on the look-ahead distance for particular varieties of lateral controllers. [16] proposed a look-ahead traffic information-based real-time MPC scheme, while [17] presented an MPC-based path-following controller with steering angle envelopes based on the look-ahead distance varying with the velocity.

Researchers have agreed that the look-ahead distance must be adaptable consequent to the variation of vehicle dynamics and environmental situations, however, opinions emerged on the adapting method and the considered factors. [18] presented a fuzzy approach as a method to determine the look-ahead distance based on the vehicle mass and the varied velocity. Whilst other methods employed learning techniques, as in [19] using deep learning and [20] by means of reinforcement learning. In general, the most researched factors affecting the look-ahead distance are vehicle velocity and road curvature. Considering the inverse relationship between the mentioned factors, studies have decided to assess only one of them. [21] proposed a tuning strategy that adapts the look-ahead distance according to the velocity variation. [22] estimated the distance manually by analyzing the closed-loop poles at different target points, while [23] proposed a velocity-based look-ahead distance taking the system reaction time into consideration. Other studies considered tuning the look-ahead distance as a function of the curvature. Based on the Dubins path algorithm, [24] improved the PP method, by heuristically selecting a look-ahead point considering the relationship between the vehicle and the path. An extension of the PP method is proposed by [25] by replacing the employed circle with a clothoid to reduce fitting errors. [26] presented a simple feedback controller that uses vehicle lateral deviations at three look-ahead points and finally chooses one. [27] tuned the look-ahead distance by applying fuzzy logic that takes the lateral error and its changing rate as inputs.

Adapting the look-ahead distance solely based on the velocity or road curvature is not sufficient. There is a set of complex scenarios that the on-road AV can't handle. While the studies presented in the literature offer valuable insights, an additional more in-depth analysis of the effect of the look-ahead distance could potentially deepen our understanding of the subject. Moreover, it will be demonstrated that road adherence is a critical factor that should be considered in tuning the look-ahead distance. Road adherence is heavily researched due to its direct impact on stability. The reader can refer to [28,29] for adherence estimation. In this study, we considered that road adherence is accessible.

By far and to the knowledge of the authors, there is no mathematical model to define the relationship between the look-ahead distance with the velocity and the curvature, not to mention road adherence. In this paper, a study is conducted on the effect of variation in vehicle velocity, road curvature, and original examination of road adherence on the look-ahead distance. A set of rules are deducted based on qualitative analysis and demonstrated by conducting several scenarios. Based on the deducted rules, and for the first time, a mathematical explicit formulation is developed for the look-ahead distance. The qualitative explanations accompanying the rules assist to bridge the gap between abstract mathematical concepts and real-world phenomena. The deductive nature of the rules helps to ensure logical consistency, and an empirical validation is performed on the model to verify its accuracy and reliability.

The paper contributions are stated as:

- Deducting set of rules for adapting the look-ahead distance as a variation of velocity, curvature, and new consideration of road adherence.
- Establishment of an explicit mathematical formula for the look-ahead distance as a function of the considered factors.
- Development of a novel fuzzy logic approach with complex membership functions and several assigned rules to determine the look-ahead distance.
- Demonstrating the capability of reducing vehicle energy consumption and enhancing stability by properly adapting the look-ahead distance.

The rest of the paper is structured as follows: Section 2 introduces the lateral control based on the look-ahead distance and deducts a set of rules based on qualitative analysis. Section 3 develops the mathematical formula for the look-ahead distance as a function of the considered factors. Section 4 presents the fuzzy logic approach for adapting the look-ahead distance. The simulation results are conducted in Section 5, followed by a conclusion in Section 6.

## 2. Look-ahead distance-based lateral control

Autonomous vehicles driven based on look-ahead systems have been the subject of research over the past three decades. Such systems operate by attempting to control the future state of the vehicle. The reason behind the inability to control the actual state is the real-time execution of the control process. Due to: 1) the non-holonomic constraint of the on-road vehicle, 2) the limitations on the maximum admissible steering angle, and 3) the tire-road dynamic model, the instantaneous minimization of the center of gravity lateral offset from the reference road is beyond the reach to attain. Therefore, lateral control is executed at a look-ahead distance $Ls$ in front of the autonomous vehicle as shown in Figure 1.

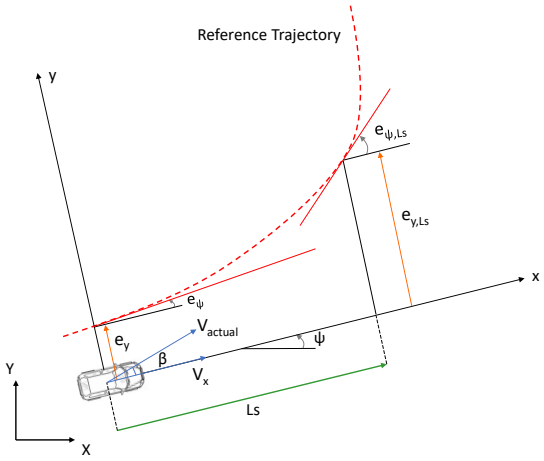


Figure 1.: Look-ahead distance illustration

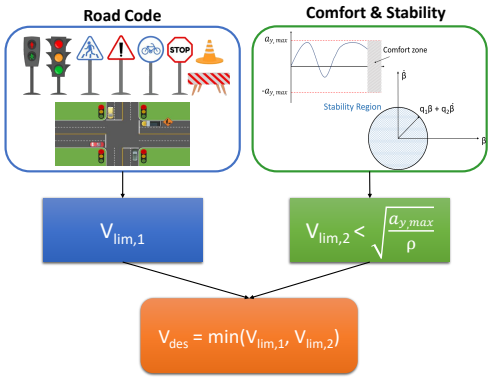


Figure 2.: Reference velocity profile

### *2.1. Lateral control*

Following the perception of the environment, the autonomous vehicle predicts the upcoming motion of the detected obstacles, selects a path, and refines it to account for the changes in the environment. The stated steps fall within the field of trajectory planning of the autonomous vehicle. Considering a pre-planned trajectory, the aim of achieving automated driving lies in controlling the lateral dynamics that ensure a trajectory following. Lateral control is realized by controlling the steering angle $\delta_c$ using the Active Front Steering (AFS) mechanism. $\delta_c$ is controlled in such a manner to minimize the lateral displacement error computed at a target point at a look-ahead distance from the vehicle ($e_{y,Ls}$), (see Figure 1).
Lateral control is associated with longitudinal control to provide comfortable driving and respects the road rules. Hence, the longitudinal velocity is controlled to track a generated reference velocity profile $V_{x,des}$ given by (1) and illustrated in Figure 2. Note that the stability region is determined based on the side-slip angle $\beta$ and its rate $\dot{\beta}$.

$$V_{x,des} = \min\left(\sqrt{\frac{a_{y,max}}{\rho}}, V_{x,lim}\right) \tag{1}$$

where $V_{x,lim}$ is the limitation according to road code, $\rho$ is the road curvature, and $a_{y,max}$ is the maximum allowable lateral acceleration to maintain comfort as defined in [30]. Therefore, lateral and longitudinal dynamics are controlled using the super-twisting sliding mode control.

#### *2.1.1. Super-Twisting Sliding Mode (STSM) control*

The Super-Twisting algorithm is a second-order sliding mode control. In spite of perturbations, it generates the continuous control function that drives the sliding variable and its derivative to reach a sliding surface during a finite time.
Consider the second-order system:

$$\ddot{x} = f(X,t) + g(X,t)u(t) \tag{2}$$

where $X = [x, \dot{x}]^T \in \mathbb{R}^2$ is the state vector, u is the control input, and f, g are continuous functions. $X_{des}$ is the desired state of X, with $X_{des} = [x_{des}, \dot{x}_{des}]^T \in \mathbb{R}^2$. The error vector E is given by $E = X - X_{des} = [e, \dot{e}]^T \in \mathbb{R}^2$ where $e = x - x_{des}$ and $\dot{e} = \dot{x} - \dot{x}_{des}$. Hence, a sliding variable with a relative degree equal to one with respect to the control input is defined :

$$s = \dot{e} + ke \tag{3}$$

The second-order derivative is given by:

$$\ddot{s}(s,t) = \Phi(s,t) + \xi(s,t)\dot{u}(t), \tag{4}$$

where $\Phi(s,t)$ and $\xi(s,t)$ are bounded functions. The goal of the Super-Twisting algorithm is to enforce the sliding variable s to converge to zero in finite time. Assume that there exist $S_0$, $b_{min}$, $b_{max}$, $C_0$, $U_{max}$ verifying that for all x $\in \mathbb{R}^n$ and $|s(x,t)| < S_0$:

$$\begin{cases} |u(t)| \leq U_{max} \\ |\Phi(s,t)| < C_0 \\ 0 < b_{min} \leq |\xi(s,t)| \leq b_{max} \end{cases} \tag{5}$$

The control input based on the Super-Twisting Sliding Mode algorithm is given as:

$$u(t) = u_1 + u_2 \begin{cases} u_1 = -\alpha_1 |s|^\tau sign(s), \tau = ]0, 0.5] \\ \dot{u}_2 = -\alpha_2 sign(s) \end{cases} \tag{6}$$

where $\alpha_1$ and $\alpha_2$ are positive gains. The following conditions guarantee the finite time convergence:

$$\begin{cases} \alpha_1 \geq \sqrt{\frac{4C_0(b_{max}\alpha_2 + C_0)}{b_{min}^2(b_{min}\alpha_2 - C_0)}} \\ \alpha_2 > \frac{C_0}{b_{min}} \end{cases} \tag{7}$$

Refer to [31] for the convergence analysis. An approximation function $\frac{s}{|s|+\epsilon}$ is used to smooth the sign(s) function, where $\epsilon > 0$.

### *2.1.2. Control problem formulation*

Two decentralized controllers are developed based on the STSM control for lateral and longitudinal control. Define the following sliding variables as

$$s_y = \dot{e}_{y,Ls} + k_y e_{y,Ls}; \text{ with } k_y > 0 \tag{8a}$$

$$s_x = (V_x - V_{x_{des}}) + k_x \int (V_x - V_{x_{des}})\, dt; \text{ with } k_x > 0 \tag{8b}$$

where $s_y$ and $s_x$ have a relative degree equal to 1 w.r.t their corresponding control inputs $\delta_c$ (steering angle) and $T_m$ (total traction torque) respectively. Hence,

$$\ddot{s}_y(s_y,t) = \Phi_y(s_y,t) + \xi_y(s_y,t)\dot{\delta}_c(t) \tag{9a}$$

$$\ddot{s}_x(s_x,t) = \Phi_x(s_x,t) + \xi_x(s_x,t)\dot{T}_m(t) \tag{9b}$$

where $\Phi_i(s_i,t)$ and $\xi_i(s_i,t)$ with $i = \{y,x\}$ are bounded functions satisfying conditions of (5). Therefore, the control inputs corresponding respectively to lateral and longitudinal control are given by

$$\delta_c = -\alpha_{\delta_c,1}|s_y|^{\tau_{\delta_c}} sign(s_y) - \alpha_{\delta_c,2}\int_0^t sign(s_y)\,d\tau, \tag{10a}$$

$$T_m = -\alpha_{T_m,1}|s_x|^{\tau_{T_m}} sign(s_x) - \alpha_{T_m,2}\int_0^t sign(s_x)\,d\tau \tag{10b}$$

where $\alpha_{\delta_c,i}$, $\alpha_{T_m,i}$ with i = [1,2] are positive constants satisfying conditions (7) and $\tau_{\delta_c}$, $\tau_{T_m}$ are constants in the interval ]0,0.5]. The STSM control inputs $\delta_c$ (10a), $T_m$ (10b) respectively guarantee the convergence of $s_y$, $s_x$ to zero in a finite time $\big(\dot{e}_{y,Ls} + k_y e_{y,Ls} \to 0$, $V_x - V_{x_{des}} + k_x\int(V_x - V_{x_{des}}) \to 0\big)$. Once reaching the sliding surface, $e_{y,Ls}$ converges exponentially to zero with a rate $k_y > 0$.

### *2.2. Adaptation rules*

The necessity for lateral control to be executed at a look-ahead distance instead of the vehicle's center of gravity has been illustrated. However, although several works proposed a constant look-ahead distance path-tracking as in [32] and [33], the constant tuning won't cover except a small part of the situations encountered by the on-road vehicle. Distinct studies presented in the literature have proposed to tune $Ls$ as a variation of velocity or curvature. The presented works lack generalities and are insufficient to cover on-road situations. Hence, in this section, we will deduct a qualitative analysis to establish a set of rules for adapting $Ls$ as a combined variation of velocity and curvature, and demonstrate the exigency of contemplating road adherence as a decisive factor to adapt $Ls$.

#### *2.2.1. Longitudinal velocity $V_x$*

Look-ahead systems compute the lateral displacement error in front of the vehicle using perceptual data derived from vision-based sensors such as cameras and LiDARs. The existing time delays in sensor measurements, controller computations, and actuator realization restrain the look-ahead distance from maintaining a velocity-independent value. The actuator may be unable to minimize the lateral error as the velocity increases if $Ls$ is unregulated. $Ls$ will be adapted to $V_x$ according to a compromise between vehicle energy consumption and the lateral error. Figure 3-(a) shows that incrementing $Ls$ results in a shorter traveled distance compared to small $Ls$ for the same target point. A shorter distance to be traveled consequently implies lower energy consumption. However, $Ls$ must not be excessively increased in order to stay in the zone of low lateral error and to allow a reasonable time for obstacle detection. Therefore as the velocity increases, $Ls$ should be increased accordingly and limited by an upper bound $Ls_{max_V}$ depending on the velocity.

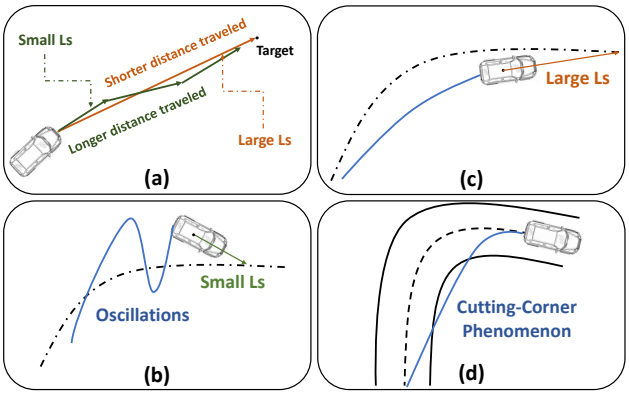


Figure 3.: Effect of $Ls$ variation

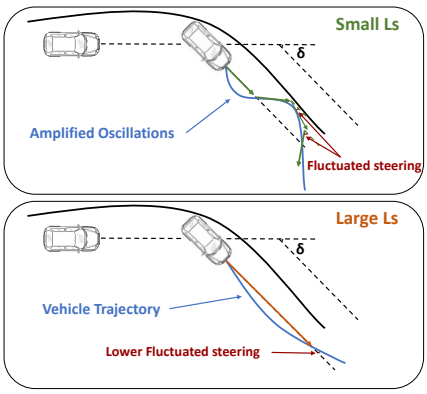


Figure 4.: Effect of adherence on $Ls$

### *2.2.2. Road curvature $\rho$*

The road is represented by a sequence of waypoints and modeled by a parametric curve. The curvature at each point on the candidate path is calculated based on the waypoints and the curvature profile with respect to a local curvilinear coordinate system. Road curvature highly influences the strategy for regulating $Ls$. In the case of an improper adaptation, lateral control deteriorates when setting target points too far from the reference road. The vehicle is forced to track the path more precisely when $Ls$ is small however it initiates oscillations yielding to instability (Figure 3-(b)). Conversely, large $Ls$ reduces overshoot and averts the oscillations (Figure 3-(c)), though if it exceeds a certain limit, it results in a high lateral error and certain phenomena such as the cutting-corner (Figure 3-(d)). Therefore, as road curvature increases, $Ls$ is decreased accordingly to enhance lateral control and avoid the cutting corner problem. Contrariwise, as $\rho$ decreases, $Ls$ is increased correspondingly to obviate the oscillations and achieve energy economy, yet adheres to a maximum threshold $Ls_{max_\rho}$.

### *2.2.3. Road adherence $\mu$*

Road adherence refers to the ability of vehicle tires to maintain proper contact and traction with the surface of the road, i.e. tire-road friction. The relation between the lateral acceleration $a_y$ with the yaw rate $\dot{\psi}$ and the side-slip angle rate $\dot{\beta}$ is given in (11), where $a_y$ is maintained below a threshold depending on $\mu$ as it directly affects lateral stability [30]. Hence, in order to preserve stability, the maximal allowable lateral acceleration decreases as road slippery increases ($\mu$ decreases).

$$a_y = V_x(\dot{\psi} + \dot{\beta}) \leq \mu g \tag{11}$$

The oscillations resulting from small $Ls$ are amplified on low-adherence roads as a result of low tire-road friction, subsequently leading to a higher side-slip angle and automatically higher lateral acceleration. Hence, to maintain stability, $Ls$ should be adapted to have higher values in the case of low-adherence roads. Define two values $Ls_{min_\mu}$, $Ls_{max_\mu}$ representing the minimum and maximum limits of $Ls$ on low-adherence roads respectively. $Ls$ is adapted to $\mu$ as a variation of $\rho$.
As $\mu$ decreases on low-curvature roads, it is preferable to reduce the look-ahead distance in order to minimize utmost the lateral error to avoid unnecessary road divergence. Though, $Ls$ should be maintained above a lower boundary that takes the

Table 1.: Look-ahead distance adaptation to $V$, $\rho$, $\mu$

| Parameter Variation | Look-ahead distance $Ls$ |
|---|---|
| $V \nearrow$ | Ls $\nearrow$ until $Ls_{max_V}$ – for dry roads – |
| $\rho \searrow$ | Ls $\nearrow$ until $Ls_{max_\rho}$ – for dry roads – |
| $\mu \searrow$ to $\leq \overline{\mu}$ | Ls $\nearrow$ to the range $[Ls_{min_\mu}, Ls_{max_\mu}]$ and depending on $\rho$ |
| $\mu \searrow$ and $\rho \searrow$ | Ls $\searrow$ until $Ls_{min_\mu}$ and $Ls_{min_\mu} \nearrow$ as $\mu \searrow$ |
| $\mu \searrow$ and $\rho \nearrow$ | Ls $\nearrow$ until $Ls_{max_\mu}$ and $Ls_{max_\mu} \nearrow$ as $\mu \searrow$ |

tracking oscillations into consideration. Hence, on low-adherence roads, as $\rho$ decreases to the minimum, $Ls$ is assigned as $Ls_{min_\mu}$, where $Ls_{min_\mu}$ increases as $\mu$ decreases. Conversely, for high-curvature roads, the vehicle is subjected to steering angle $\delta$ to track the desired path. Thus, an additional fluctuating steering reflected by the tracking oscillations to $\delta$ results in a large lateral error and imposes a high lateral acceleration, leading to vehicle instability (see Figure 4). Hence, $Ls$ should be increased in this case. Therefore, on low-adherence roads, as $\rho$ increases to the maximum, $Ls$ is assigned as $Ls_{max_\mu}$, where $Ls_{max_\mu}$ increases as $\mu$ decreases.

Table 1 summarizes the rules for adapting $Ls$ to $V, \rho$ and $\mu$ depending on $\rho$, where $Ls_{max_V}$, $Ls_{max_\rho}$ present a compromise between energy consumption and path-tracking accuracy and respect the road rules, $Ls_{min_\mu} > \max\{Ls_{max_\rho}, Ls_{max_V}\}$, and $\{Ls_{min_\mu}$, $Ls_{max_\mu}\}$ increase as $\mu$ decreases. Note that the low and high thresholds for the parameters are defined in the next section.

## 3. Explicit function formulation

In this section, a mathematical formulation is established for the look-ahead distance as a function of the velocity $V$, curvature $\rho$, and adherence $\mu$. The parameters of the developed function abide by the rules deducted in the previous section. The formula of the function is derived by drawing inspiration from the following principles: 1) nonlinear relationship to capture intricate dependencies, 2) continuity and differentiability, 3) boundedness and saturation to confine the output within specific limits, and 4) incorporation of a modifiable smooth transition state to allow flexibility in adjusting its behavior.

### *3.1. Function of velocity and curvature*

Let $f_1$ be a function of the longitudinal velocity $V$ such that

$$f_1(V) = \xi_1 \frac{1}{1 + e^{-\frac{2\gamma_1}{\overline{V}-\underline{V}}(V - \frac{\overline{V}+\underline{V}}{2})}} + \xi_2, \tag{12}$$

where $\xi_1, \xi_2$ are shaping parameters for $f_1$, $\underline{V}$ and $\overline{V}$ are the extremities of the transient state of $f_1$, and $\gamma_1$ represents the intensity of the slope of the transients-state centroid

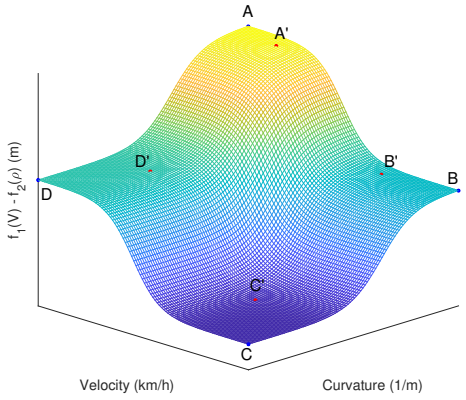


Figure 5.: Reshaping Points

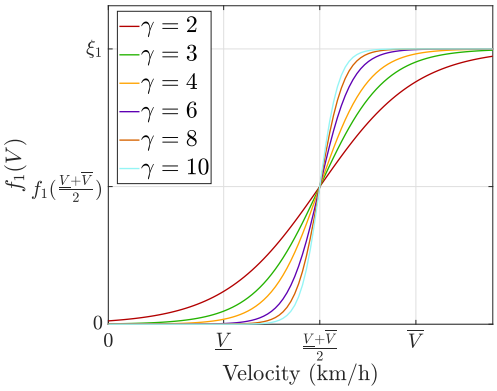


Figure 6.: $f_1(V)$ as $\gamma$ varies

of $f_1$. Similarly, let's define $f_2$ to be a function of the road curvature $\rho$,

$$f_2(\rho) = \zeta_1 \frac{1}{1 + e^{-\frac{2\gamma_2}{\overline{\rho}-\underline{\rho}}(\rho - \frac{\overline{\rho}+\underline{\rho}}{2})}} + \zeta_2, \tag{13}$$

where $\zeta_1$, $\zeta_2$ are shaping parameters for $f_2$, $\underline{\rho}$ and $\overline{\rho}$ are the extremities of the transient state of $f_2$, and $\gamma_2$ represents the intensity of the slope of the transients-state centroid of $f_2$. Following the deducted rules for the look-ahead distance, $Ls$ must increase with velocity increasing, and conversely increase with the decrease of curvature, both under a limited threshold. Hence, we can formulate $Ls$ as a function of velocity and curvature as follows:

$$Ls(V, \rho) = f_1(V) - f_2(\rho) \tag{14}$$

In order to reshape the proposed function, one has to determine the 10 unknown parameters: $\xi_i$, $\zeta_i$, $\gamma_i$ and $\overline{\rho}, \underline{\rho}$, $\overline{V}, \underline{V}$ where $i = [1, 2]$. $\xi_i$ and $\zeta_i$ comprise the location of the four extremities of the function while the remnant parameters constitute the characteristics of the sigmoid functions. To this end, let A($V_{max}$, 0), B(0,0), C(0,$\rho_{max}$), and D($V_{max}$,$\rho_{max}$) denote the function extremities (Figure 5), and let $\xi_3 = \xi_2 - \zeta_2$. Then, the look-ahead distance at these points can be formulated as

$$Ls_A = \left[\frac{1}{1 + e^{-\frac{2\gamma_1}{\overline{V}-\underline{V}}(V_{max} - \frac{\overline{V}+\underline{V}}{2})}}\right]\xi_1 - \left[\frac{1}{1 + e^{\gamma_2 \frac{\overline{\rho}+\underline{\rho}}{\overline{\rho}-\underline{\rho}}}}\right]\zeta_1 + \xi_3 \tag{15a}$$

$$Ls_B = \left[\frac{1}{1 + e^{\gamma_1 \frac{\overline{V}+\underline{V}}{\overline{V}-\underline{V}}}}\right]\xi_1 - \left[\frac{1}{1 + e^{\gamma_2 \frac{\overline{\rho}+\underline{\rho}}{\overline{\rho}-\underline{\rho}}}}\right]\zeta_1 + \xi_3 \tag{15b}$$

$$Ls_C = \left[\frac{1}{1 + e^{\gamma_1 \frac{\overline{V}+\underline{V}}{\overline{V}-\underline{V}}}}\right]\xi_1 - \left[\frac{1}{1 + e^{-\frac{2\gamma_2}{\overline{\rho}-\underline{\rho}}(\rho_{max} - \frac{\overline{\rho}+\underline{\rho}}{2})}}\right]\zeta_1 + \xi_3 \tag{15c}$$

$$Ls_D = \left[\frac{1}{1 + e^{-\frac{2\gamma_1}{\overline{V}-\underline{V}}(V_{max} - \frac{\overline{V}+\underline{V}}{2})}}\right]\xi_1 - \left[\frac{1}{1 + e^{-\frac{2\gamma_2}{\overline{\rho}-\underline{\rho}}(\rho_{max} - \frac{\overline{\rho}+\underline{\rho}}{2})}}\right]\zeta_1 + \xi_3 \tag{15d}$$

To provide an exact set of values for the function extremities, the reshaping should be performed at points A, B, C, and D. However, this configuration following (15)

depends on the transient-state extremities $\underline{\rho}$, $\overline{\rho}$, $\underline{V}$, $\overline{V}$ with exact providing of the boundaries for $Ls$ ($V_{max}$, $\rho_{max}$). To avoid this, the reshaping will be performed at the extremities of the transient state of the sigmoid functions. Hence, the look-ahead distance at A'($\overline{V}$, $\underline{\rho}$), B'($\underline{V}$, $\underline{\rho}$), C'($\underline{V}$,$\overline{\rho}$), and D'($\overline{V}$,$\overline{\rho}$) can be given by:

$$Ls_{A'} = \Big[\frac{1}{1+e^{-\gamma_1}}\Big]\xi_1 - \Big[\frac{1}{1+e^{\gamma_2}}\Big]\zeta_1 + \xi_3 \tag{16a}$$

$$Ls_{B'} = \Big[\frac{1}{1+e^{\gamma_1}}\Big]\xi_1 - \Big[\frac{1}{1+e^{\gamma_2}}\Big]\zeta_1 + \xi_3 \tag{16b}$$

$$Ls_{C'} = \Big[\frac{1}{1+e^{\gamma_1}}\Big]\xi_1 - \Big[\frac{1}{1+e^{-\gamma_2}}\Big]\zeta_1 + \xi_3 \tag{16c}$$

$$Ls_{D'} = \Big[\frac{1}{1+e^{-\gamma_1}}\Big]\xi_1 - \Big[\frac{1}{1+e^{-\gamma_2}}\Big]\zeta_1 + \xi_3 \tag{16d}$$

Beyond A', B', C', and D', the function saturates and the correspondent values for $Ls$ are close to that at A, B, C, and D. Let $f_1$ and $f_2$ have the same value of slope intensity of the centroid ($\gamma_1 = \gamma_2 = \gamma$) and denote $\mathcal{B}$ the desired values for reshaping A', B', and C'. The aim is to find $\xi_1, \xi_3 (= \xi_2 - \zeta_2)$ and $\zeta_1$ as a function of $\gamma$. Thus,

$$\mathcal{A} = \begin{bmatrix} \frac{1}{1+e^{-\gamma}} & 1 & -\frac{1}{1+e^{\gamma}} \\ \frac{1}{1+e^{\gamma}} & 1 & -\frac{1}{1+e^{\gamma}} \\ \frac{1}{1+e^{\gamma}} & 1 & -\frac{1}{1+e^{-\gamma}} \end{bmatrix};\ \mathcal{B} = \begin{bmatrix} Ls_{A'} \\ Ls_{B'} \\ Ls_{C'} \end{bmatrix} = \begin{bmatrix} b_1 \\ b_2 \\ b_3 \end{bmatrix};\ X = \begin{bmatrix} \xi_1 \\ \xi_3 \\ \zeta_1 \end{bmatrix} \tag{17}$$

The formulated problem $\mathcal{A}X = \mathcal{B}$ is solved using the Gaussian elimination method. $X^* = [\xi_1^*\ \xi_3^*\ \zeta_1^*]^T$ can be determined by an iterative solution as follows:

$$\zeta_1^* = (b_3 - b_2)\frac{(1+e^{-\gamma})(1+e^{\gamma})}{e^{-\gamma} - e^{\gamma}} \tag{18a}$$

$$\xi_3^* = \frac{1}{e^{\gamma} - e^{-\gamma}}\Big[-(1+e^{-\gamma})b_1 + (1+e^{\gamma})b_2 - \frac{e^{-\gamma} - e^{\gamma}}{1+e^{\gamma}}\zeta_1^*\Big] \tag{18b}$$

$$\xi_1^* = (1+e^{-\gamma})(b_1 + \frac{1}{1+e^{\gamma}}\zeta_1^* - \xi_3^*) \tag{18c}$$

The derivative of $f_1(V)$ at the centroid is given by

$$f'_{1(\frac{\overline{V}+\underline{V}}{2})} = \frac{df_1}{dV}|_{\frac{\overline{V}+\underline{V}}{2}} = \frac{\xi_1\gamma}{2(\overline{V} - \underline{V})} \tag{19}$$

Figure 6 shows the variation of transient-state intensity as a variation of $\gamma$. As $\gamma$ tends to $\infty$, the tangent line at the centroid becomes vertical. As the intensity of the slope depends also on $\overline{V}$ and $\underline{V}$, the angle of the slope with the V-axis could be obtained using (19) by proper choice for $\overline{V} - \underline{V}$; similarly, for $f_2$ and $\overline{\rho} - \underline{\rho}$.
From Figure 6, choose $\gamma = 4$ for $f_1$ and $f_2$. Then the shaping parameters can be solved using (18) and given by $X = \begin{bmatrix}5.1866 & 5.9907 & 4.6679\end{bmatrix}^T$. Finally, after assigning the parameters $\overline{V} = 80\ km/h$, $\underline{V} = 30\ km/h$, $\overline{\rho} = 0.02\ m^{-1}$ and $\underline{\rho} = 0.002\ m^{-1}$, the look-ahead distance function of velocity and curvature $f_1(V) - f_2(\rho)$ can be seen in Figure 7.

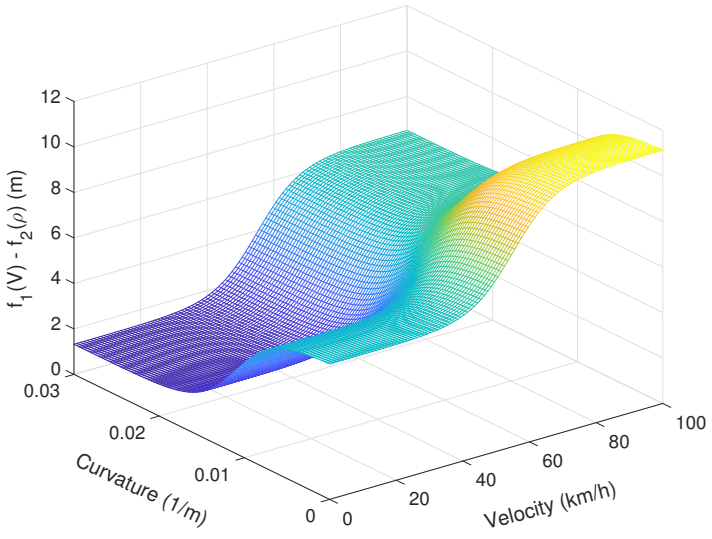


Figure 7.: $Ls$ function of velocity $V$ and curvature $\rho$: $f_1(V) - f_2(\rho)$

### *3.2. Function of adherence and curvature*

Look-ahead distance must be adapted with road adherence depending on curvature variation as stated in the adaptation rules. However, this relationship is more complex than a combined sum of two functions of a single variable.
Therefore, let's define a new function $f_3$ representing the correlation of the look-ahead distance with road curvature and adherence as

$$f_3(\mu, \rho) = k_1(\mu)k_2(\rho) \times \lambda_{adapt}, \tag{20}$$

where,

$$k_1(\mu) = 1 - \frac{1}{1 + e^{-\frac{\chi_1}{(\overline{\mu}-\underline{\mu})/2}(\mu - \frac{\overline{\mu}+\underline{\mu}}{2})}} \tag{21a}$$

$$k_2(\rho) = \frac{1}{1 + e^{-\frac{\chi_2}{(\overline{\rho}-\underline{\rho})/2}(\rho - \frac{\overline{\rho}+\underline{\rho}}{2})}} \tag{21b}$$

where $\chi_1$, $\overline{\mu}$, $\underline{\mu}$ and $\chi_2$, $\overline{\rho}$, $\underline{\rho}$ represent the intensity of the slope of the transients-state centroid and the extremities of the transient-state for the functions $k_1(\mu)$ and $k_2(\rho)$ respectively. $\lambda_{adapt}$ is an adaptation gain to provide an upper bound for $f_3$.
let M be a point of coordinates $(\underline{\mu}, \overline{\rho})$ and c the desired value for $Ls$ at M. Hence $f_3|_M$ is given by

$$f_3|_M = f_3(\underline{\mu}, \overline{\rho}) = \left[1 - \frac{1}{1 + e^{\chi_1}}\right]\left[\frac{1}{1 + e^{-\chi_2}}\right]\lambda_{adapt} = \iota \tag{22}$$

Let $k_1(\mu)$ and $k_2(\rho)$ have the same intensity of slope, meaning $\chi_1 = \chi_2 = \chi$. Hence,

$$\lambda_{adapt} = \iota \, \frac{(1 + e^{\chi})(1 + e^{-\chi})}{e^{\chi}} \tag{23}$$

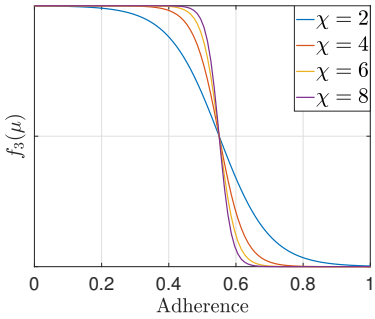


Figure 8.: $f_3(\mu)$ as $\chi$ varies

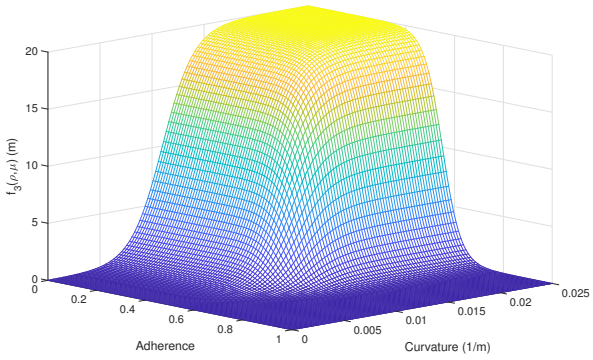


Figure 9.: $Ls$ Function $f_3(\rho, \mu)$

Figure 8 shows the variation of the behavior of $f_3(\mu)$, for a fixed $\rho$, as $\chi$ increases. Hence, by choosing $\chi = 4$, assigning the desired value $\iota = 20$ at $\mathrm{M}(\underline{\mu}, \overline{\rho})$, and defining $\underline{\mu} = 0.4$ and $\overline{\mu} = 0.7$, the look-ahead distance function of adherence and curvature $\overline{f_3}$ is given in Figure 9. Note that $f_3$ assists $Ls$ by additional gain only when the adherence is low, i.e. if $\mu = 1$, $f_3$ will be zero independent of the value of $\rho$.

Therefore, the look-ahead distance final formulation can be represented by

$$Ls(V, \rho, \mu) = f_1(V) - f_2(\rho) + f_3(\mu, \rho) \tag{24}$$

Note that the calculated parameters are completely tunable. The objective was to develop a generalized formulation for real-time continuous implementation of the look-ahead distance in dependence on several computable parameters. The shaping parameters $\xi_i$, $\zeta_i$, $\gamma_i$, $\chi_i$ and $\lambda_{adapt}$ with $i = [1, 2]$ are highly dependent on the desired objectives and the developed controller. The variation of the response time and feedback gain in the controller type may require variation in the look-ahead distance range, the rate of variation of the transient state, or limitation of the bounds. Further, the range of variation of $Ls$ depends on the desired objectives. A low range bestows better path-tracking at the cost of energy consumption, and vice versa.
Therefore, the developed formula is designed in a generalized manner, and it is independent of the vehicle parameters. Its tuning relies on the controller's characteristics such as gain and response time, as well as the specific objectives to be achieved. This attribute showcases a prominent edge, where the foremost advantage of this formula lies in its inherent reproducibility, allowing it to be easily replicated and applied.

Based on the defined adaptation rules, another strategy is developed based on a fuzzy logic approach to be contrasted with the developed continuous function.

## 4. Fuzzy logic decision approach

Fuzzy logic employs a set of rules based on expert knowledge to reach the fuzzy decision conveyed by linguistic values. The fuzzy logic system consists of three stages: Fuzzification, Inference Engine, and Defuzzification [34]. Based on the shape of the membership functions, linguistic inputs are generated from crisp ones by computing

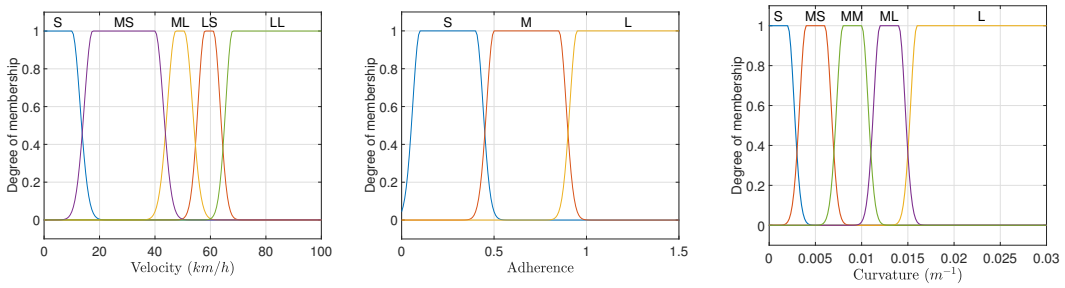


Figure 10.: Fuzzy Logic Inputs: $V$, $\mu$, and $\rho$

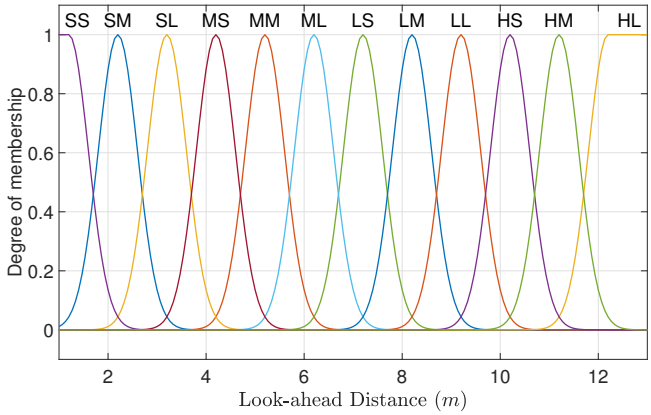


Figure 11.: Fuzzy Logic Output: $Ls$

the relative degree of truth during the Fuzzification process. The membership functions for the velocity $V$, curvature $\rho$, and adherence $\mu$ are shown in Fig. 10. These functions are defined as a combination of Gaussian functions to provide a smooth variation, where each Gaussian function is represented by (25).

$$f = e^{(-\frac{(x-c)^2}{2\sigma^2})}, \tag{25}$$

where c is the mean and $\sigma$ represents the standard deviation. Five fuzzy sets are defined for the velocity V: {Small (S), Medium-Small (MS), Medium-Large (ML), Large-Small (LS), Large-Large (LL)}. Three fuzzy sets for the adherence $\mu$: {Small (S), Medium (M), Large (L)}, and five sets for the curvature $\rho$: {Small (S), Medium-Small (MS), Medium-Medium (MM), Medium-Large (ML), Large (L)}. The Rule Base in the Inference Engine is established based on the driver's experience and multiple conducted simulations and abides by the deducted adaptation rules. Rules are defined in terms of two parameters ($V$, $\rho$) for each set of $\mu$, and divided into 3 tables shown in Tables 2, 3, 4. Hence, for each set of values for the inputs ($V$, $\rho$, $\mu$), there exists one value for the output $Ls$. The fuzzy implication is solved using the [35] inference method (min-min-max). The membership functions of the output fuzzy variable $Ls$ are given in Fig. 11, in the form of Gaussian functions (25). Twelve sets are defined for the look-ahead distance $Ls$: {ij} where $i$: {Small (S), Medium (M), Large (L), Huge (H)} and $j$: {Small (S), Medium (M), Large (L)}, and the centroid method is used for the Defuzzification process.

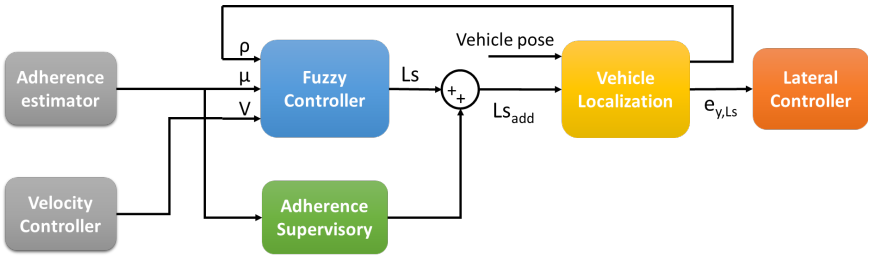


Figure 12.: Fuzzy control scheme

| | | V | | | | |
|---|---|---|---|---|---|---|
| | **Ls** | S | MS | ML | LS | LL |
| | S | ML | LS | LM | LL | HS |
| | MS | MM | ML | LS | LM | LL |
| $\rho$ | MM | MS | MM | ML | LS | LM |
| | ML | SL | MS | MM | ML | LS |
| | L | SM | SL | MS | MM | ML |

Table 2.: Rules for $\mu$ = L

| | | V | | | | |
|---|---|---|---|---|---|---|
| | **Ls** | S | MS | ML | LS | LL |
| | S | SL | MS | MM | ML | LS |
| | MS | MS | MM | ML | LS | LM |
| $\rho$ | MM | MM | ML | LS | LM | LL |
| | ML | ML | LS | LM | LL | HS |
| | L | LS | LM | LL | HS | HM |

Table 3.: Rules for $\mu$ = M

As shown in Figure 11, $Ls$ ranges from SS $\approx$ 1.5 to HL $\approx$ 13. However, as it will be shown later, the required look-ahead distance on extremely low-adherence high-curvature roads exceeds 20 $m$. More membership functions will render the system more complex and impose more rules. Expanding the membership functions, alternatively, will result in a greater discontinuity in $Ls$ and reflect an instability to the vehicle. In light of this, an adherence supervisory block is inserted into the system. This block generates an additional look-ahead distance $Ls_{add}$ to be combined with $Ls$ based on analyzing road adherence. $Ls_{add}$ can take several values and increases as $\mu$ decreases. Further, if $\mu$ decreases below a minimum threshold $\mu_{min}$ reflecting an extreme road condition, then the effect of varying $Ls$ dwindles. In this case, the supervisory block assigns 0 to $Ls_{add}$ and requests an emergency braking. The complete control scheme is shown in Fig. 12.

## 5. Simulation Results

The proposed approaches for the look-ahead distance are implemented on the lateral controller and validated in a joint simulation between Simulink/MatLab and SCANeR$^{TM}$ Studio vehicle dynamics simulator. The autonomous vehicle has been

| | | V | | | | |
|---|---|---|---|---|---|---|
| | **Ls** | S | MS | ML | LS | LL |
| | S | MS | MM | ML | LS | LM |
| | MS | MM | ML | LS | LM | LL |
| $\rho$ | MM | ML | LS | LM | LL | HS |
| | ML | LS | LM | LL | HS | HM |
| | L | LM | LL | HS | HM | HL |

Table 4.: Rules for $\mu$ = S

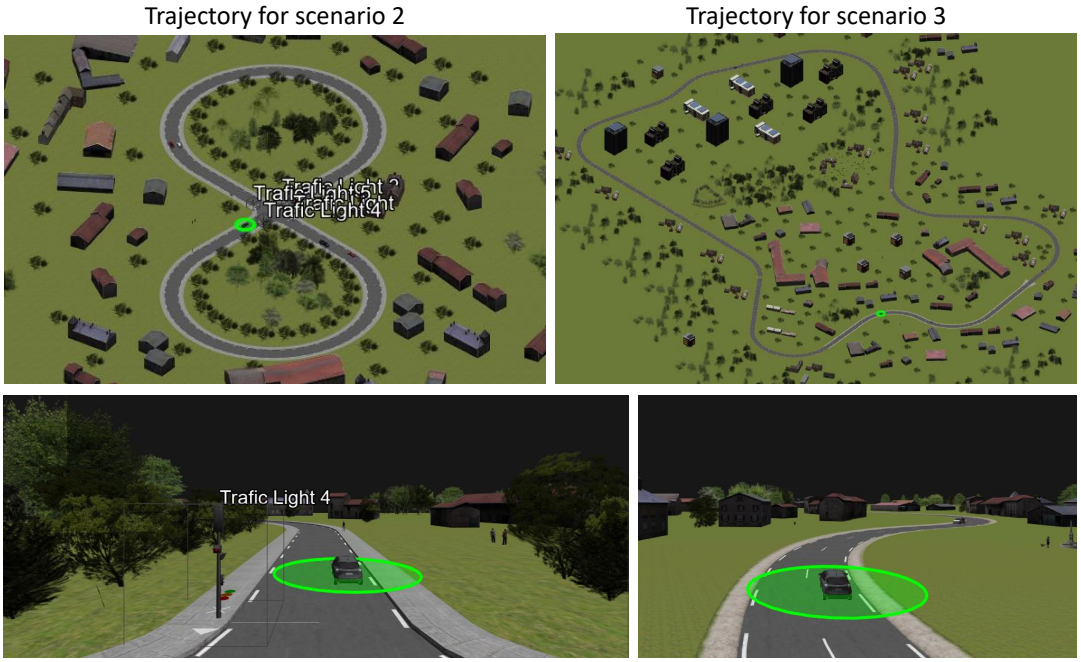


Figure 13.: SCANeR$^{\text{TM}}$ Studio simulator environment

set under several tests covering extreme road conditions. A case study is performed considering four scenarios, where each scenario presents a specific advantage of the look-ahead distance approaches. The mathematically formulated $Ls$ will be denoted by "continuous" while the fuzzy logic approach will simply be indicated by "fuzzy". The behavior of the autonomous vehicle under the continuous and fuzzy look-ahead distance will be contrasted with that using constant $Ls$. Further, it will be compared with another method we proposed for adapting $Ls$ as a sole function of velocity (26).

$$Ls = f(v) = \begin{cases} 3 & \text{if } V \leq 10/3.6 \\ 0.42V + 1.83 & \text{if } 10/3.6 \leq V \leq 70/3.6 \\ 10 & \text{if } V \geq 70/3.6 \end{cases} \tag{26}$$

where $V$ is in $m/s$ and $Ls$ in $m$. $f(v)$ is proposed as a linear function inspired from (12), reflecting a mimicked linear behavior of the proposed continuous function independent of $\rho$ and $\mu$.

### *5.1. SCANeR$^{TM}$ Studio vehicle dynamics simulator*

The proposed look-ahead distance-based lateral controller is implemented and validated in a co-simulation between Simulink/MatLab and the professional SCANeR$^{\text{TM}}$ Studio vehicle dynamics simulator. The fully dynamic vehicle "Callas" is used for testing. The Callas model consists of a full nonlinear vehicle model combining longitudinal and lateral dynamics, suspension forces, wheel dynamics, and the tire-road dynamic model. It is formed by a complex interconnection between the physical systems of the vehicle including the engine, steering system, braking, transmission, and more. This model enables the adjustment of specific vehicle properties for instance engine oil tem-

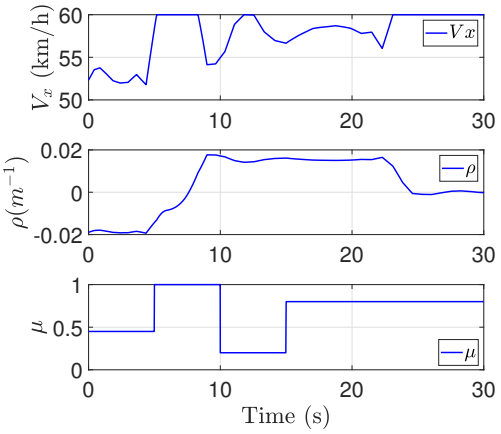


(a) Variation of $v, \rho, \mu$ - sc1

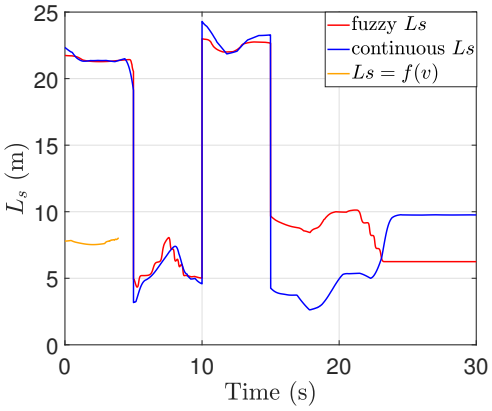


(b) Look-ahead distances - sc1

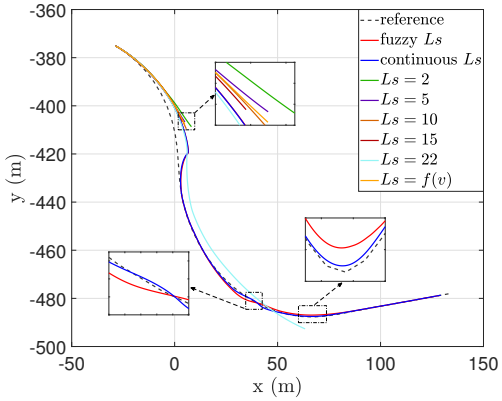


(c) Trajectories - sc1

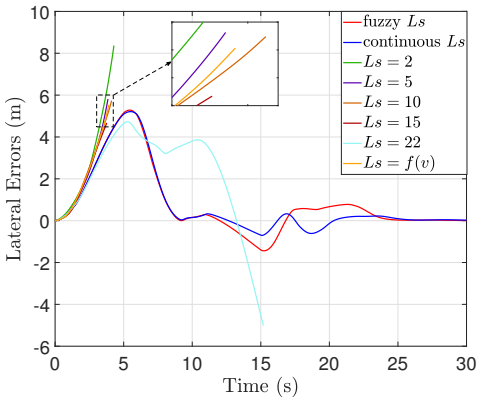


(d) Lateral errors - sc1

Figure 14.: Scenario 1 results

perature. The controlled steering angle is fed via a steering system considering a linear proportion between the steering wheel and the front wheels. The simulator offers the implementation of realistic scenarios (see Figure 13) with real-world physics (crashing, slipping, rollover, etc..).

### *5.2. Scenario 1 (sc1): Extreme adherence changing*

The first scenario is executed on a high-curvature corner under abrupt adherence variation. The varying velocity, curvature, and adherence are shown in Figure 14a. The scenario can be seen as four adherence-distinct portions under varying curvature. This extreme variation of road adherence can occur with a sudden appearance of an oily road. The fuzzy and continuous look-ahead distances are given in Figure 14b. It can be seen that $Ls$ exceeds $20\,m$ on the high-curvature low-adherence portions. The road divergence arises when the lateral error from the reference lane is large and constantly diverging and the controller is not capable of further diminishing it. Consequently, a complete loss of stability exists and the simulation is ceased. At the first portion of the test, the required $Ls$ by taking $\mu$ as an adapting factor exceeds $20m$. Hence, the constant assigning of $Ls$ for $2, 5, 10, 15\,m$ leads the AV to diverge

from the trajectory (Figure 14c) after the lateral error exceeded $6\,m$ and persists diverging (Figure 14d). Similarly, $Ls$ as a function of velocity $f(v)$ (26) ranged around $8\,m$ (Figure 14b) until it diverged. The constant appointing of $Ls$ to $22\,m$ succeeded to complete the first portion of the test as it is close to the approaches considering the adherence factor. However, in the second portion, when the adherence increased to 1, $Ls = 22\,m$ revealed a cutting corner phenomenon (Figure 14c) as it should be decreased to less than $10\,m$. Finally, the abrupt decrease in adherence to 0.3, forces the required $Ls$ to increase above $23\,m$ leading to the divergence of the autonomous vehicle. Therefore, road adherence is a decisive factor that should be considered in adapting $Ls$, in terms of stability and path-tracking of the AV. It can be noticed that only the continuous and the fuzzy $Ls$ have permitted the vehicle to complete the test, with better tracking in the continuous $Ls$ case.

### *5.3. Scenario 2 (sc2): Hard road geometry*

The second scenario is performed on the map shown in Figure 15a presenting a hard challenging geometry for lateral control. The desired velocity and the velocity of the vehicle, the road curvature, and adherence are given in Figure 15b. The adherence is kept at 1 to reveal the advantages of using the proposed approaches when the constant $Ls$ and $Ls = f(v)$ are effective. In order to have a better insight into the behavior of each approach, the following cost variables are introduced:

- Root Mean Square of the lateral error: $\sqrt{\frac{1}{\tau}\int_0^\tau e_y^2\,dt}$
- Maximum lateral error: $e_{y,max}$
- Accumulated energy consumption: $E = \int_0^{t_i} \sum_{j=1}^{4} \frac{T_j \omega_j}{\eta_j}$

where $T_j, \omega_j, \eta_j$ are respectively the torque, rotational velocity, and efficiency of the motor $j$. Note that in this work, the vehicle is electric and equipped with four in-wheel motors ($\sum_{j=1}^{4} T_j = T_m$). The strategy for torque allocation falls outside the specific scope and focus of the paper. The continuous and fuzzy $Ls$ as well as $Ls = f(v)$ are given in Figure 15c. Their corresponding lateral errors along with the constant $Ls = 2, 5, 10\,m$ are shown in Figure 15d. The constant $Ls = 10\,m$ and $Ls = f(v)$ revealed an undesirable behavior. The cost variables are determined for each approach and given in Figure 15e. $Ls = 10\,m$ revealed the maximum RMS and $e_{y,max}$, followed by $Ls = f(v)$, where both have a total energy consumption $E$ approximately as the fuzzy $Ls$. $Ls = 2\,m$ has the second least RMS after the continuous $Ls$ however with the maximum battery energy consumption. The RMS of the fuzzy $Ls$ comes between $Ls = 2\,m$ and $Ls = 5\,m$, with an energy consumption less than $Ls = 5\,m$. As for $e_{y,max}$, the fuzzy $Ls$ exhibited the minimum of all approaches, followed by $Ls = 5\,m$. The continuous $Ls$ and $Ls = 2\,m$ revealed an $e_{y,max}$ greater than $Ls = 5\,m$. Therefore, the continuous $Ls$ exhibited the minimum RMS and energy consumption and is followed by the fuzzy $Ls$, though $e_{y,max}$ is lower in the fuzzy $Ls$ case.

### *5.4. Scenario 3 (sc3): Urban environment testing*

The third scenario represents an urban map given in Figure 16a. The desired comfort-based velocity profile is determined and reduplicated by a constant of 1.2 to alienate the vehicle from its comfortable driving. In addition to the velocity, the curvature, and adherence are shown in Figure 16b. In order to compare the behavior of the fuzzy and

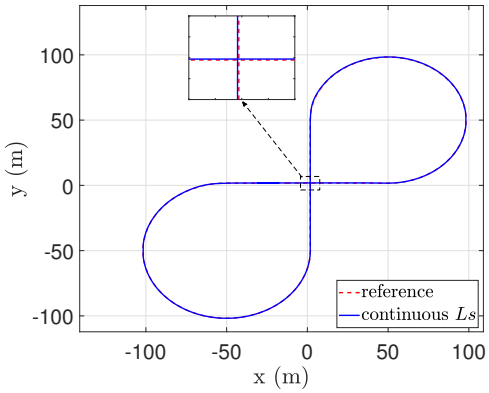


(a) Trajectory - sc2

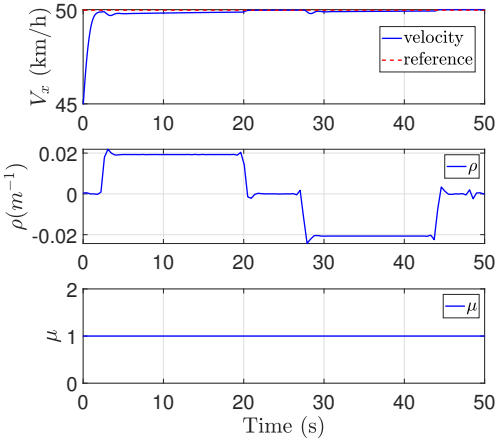


(b) Variation of $v, \rho, \mu$ - sc2

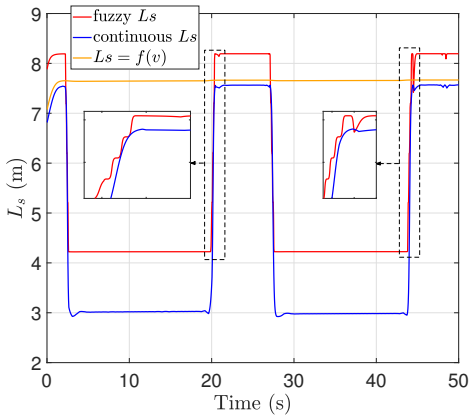


(c) Look-ahead distances - sc2

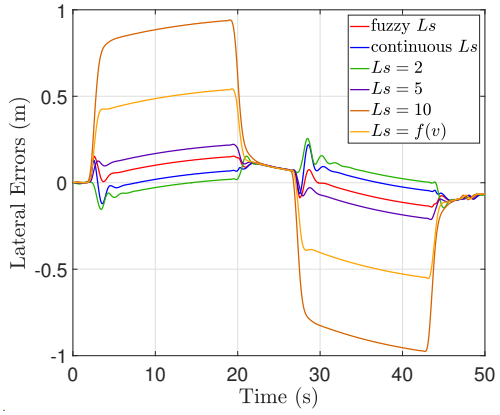


(d) Lateral errors - sc2

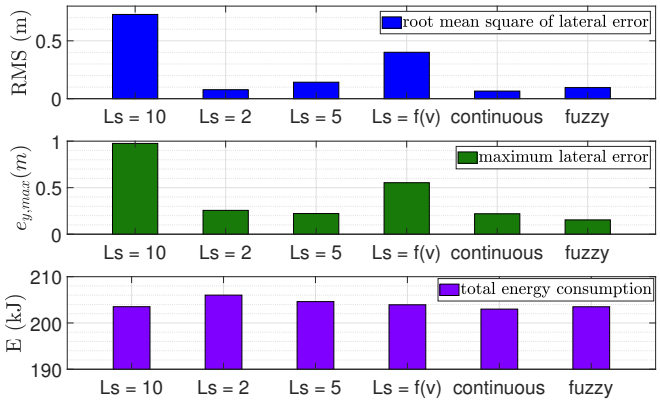


(e) Cost variables - sc2

Figure 15.: Scenario 2 results

continuous approaches in a normal daily urban environment, the adherence is kept at 1. The continuous $Ls$, fuzzy $Ls$, and $Ls = f(v)$ are determined and given in Figure 16c. The corresponding lateral errors are shown in Figure 16d along with that of the

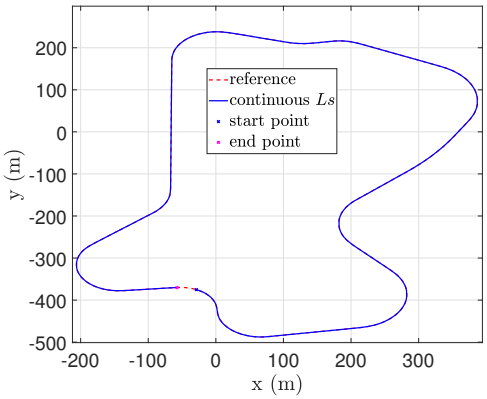


(a) Trajectory - sc3

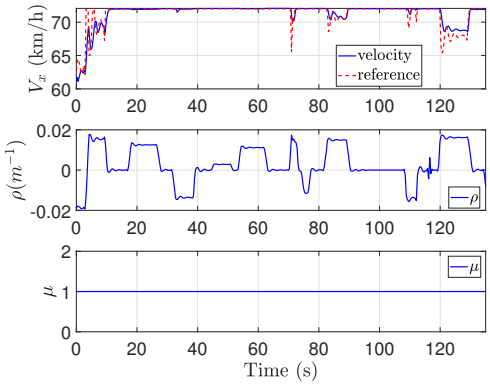


(b) Variation of $v, \rho, \mu$ - sc3

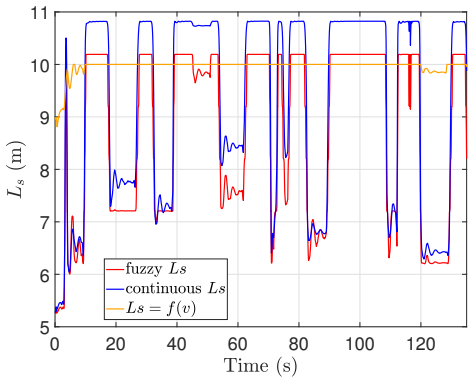


(c) Look-ahead distances - sc3

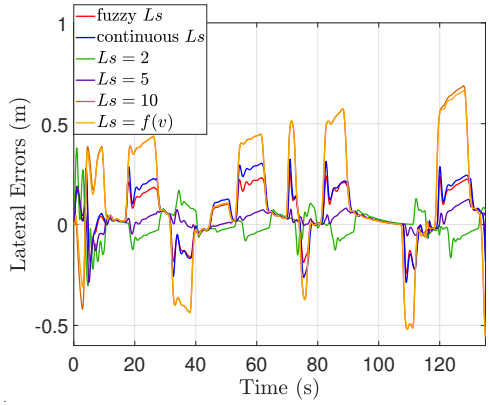


(d) Lateral errors - sc3

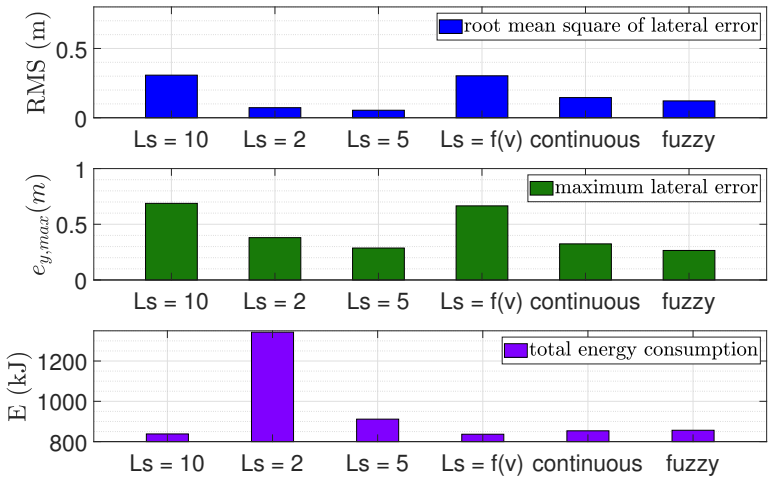


(e) Cost variables - sc3

Figure 16.: Scenario 3 results

constants $Ls = 2, 5, 10\,m$. For the sake of comparison, the cost variables are computed and given in Figure 16e. The maximum lateral error and the RMS of $Ls = 10\,m$ and $Ls = f(v)$ are the largest of all approaches, although with the lowest consumed

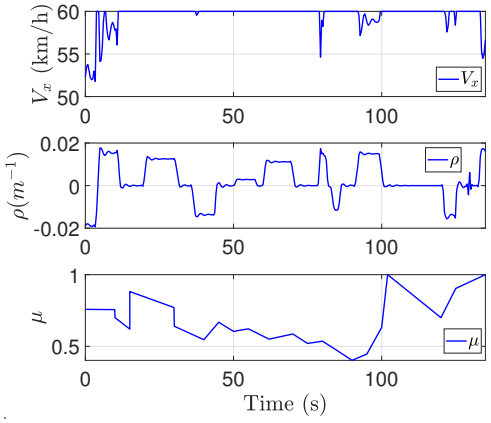


(a) Variation of $v, \rho, \mu$ - sc4

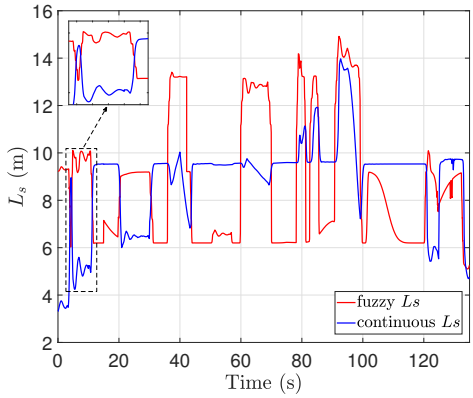


(b) Look-ahead distances - sc4

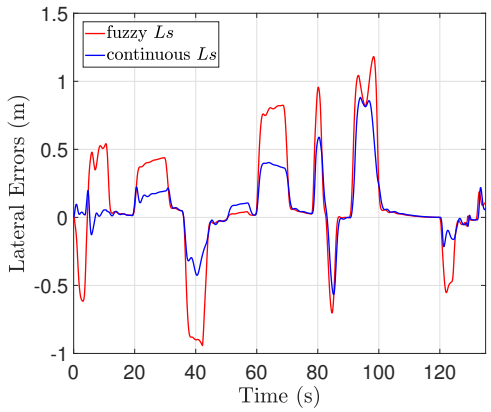


(c) Lateral errors - sc4

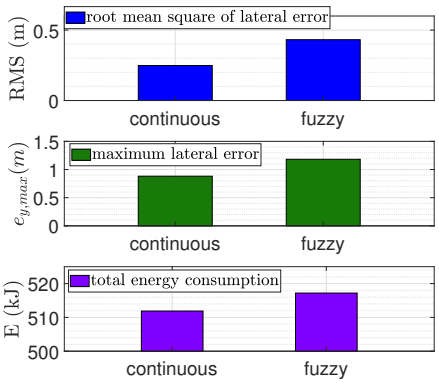


(d) Cost variables - sc4

Figure 17.: Scenario 4 results

energy. $Ls = 2\ m$ exhibited the largest energy consumption and the second least RMS after $Ls = 5\ m$. The fuzzy $Ls$ revealed an $e_{y,max}$ similar to $Ls = 5\ m$ but higher RMS. The fuzzy $Ls$ resulted in a compromise in lateral error and energy consumption between $Ls = 10\ m$ and $Ls = 5\ m$. The continuous $Ls$ revealed an energy consumption lower than the fuzzy $Ls$, however with slightly greater $e_{y,max}$ and RMS. Therefore, the continuous and fuzzy $Ls$ exhibited an optimal trade-off between path-tracking and energy consumption in daily urban environments.

### *5.5. Scenario 4 (sc4): Continuous adherence variation*

The last scenario is executed on the same trajectory as scenario 3. The desired velocity profile, road curvature, and road adherence are given in Figure 17a. The adherence is varied continuously considering mid-adherence at the beginning, followed by low adherence road portion, and finally, it increases to a high adherence portion. As the constant approach for assigning $Ls$ and the function of velocity exhibited an unacceptable behavior reflecting road divergence, only the continuous and fuzzy $Ls$ are compared in this test. The look-ahead distances for the continuous and fuzzy approaches are given in Figure 17b. In contrast to the continuous $Ls$, the discontinuity

Table 5.: Computational effort of calculating the look-ahead distance

| Scenario cases | Execution time for look-ahead distance computation (s) | | Simulation time (s) |
|---|---|---|---|
| | Fuzzy | Continuous | |
| Scenario 1 | 24.64 | 0.23 | 30 |
| Scenario 2 | 40.91 | 0.385 | 50 |
| Scenario 3 | 111.262 | 1.004 | 135 |
| Scenario 4 | 110.947 | 0.993 | 135 |

in the value transition can be noticed in the fuzzy $Ls$ (referring to the abrupt change). The presence of this disruption has an impact on the side-slip angle and, as a result, influences the vehicle's stability. Hence, a significant benefit of the continuous function lies in its ability to provide a seamless transition, thereby enhancing vehicle stability compared to the fuzzy approach. The lateral errors of the AV using the continuous and fuzzy $Ls$ are shown in Figure 17c. It is obvious that the lateral error of the continuous $Ls$ is almost always lower than that of the fuzzy $Ls$. The cost variables of the two proposed approaches are given in Figure 17d. The total energy consumption of the battery, the maximum lateral error, and the RMS of the lateral error are all lower in the continuous $Ls$ than the fuzzy one. Hence, employing the continuous function of $Ls$ yields a higher energy economy and superior path-tracking performance compared to the utilization of the fuzzy logic approach.

### *5.6. Recap*

The performed tests have revealed the major performance of the AV under the proper adaptation of the look-ahead distance of the lateral controller. It has been demonstrated that, under the same controller with the same tuning parameters, the variation of the opted strategy to adapt $Ls$ results in a diverse demeanor of the AV. Scenario 1 demonstrated the necessity of considering road adherence as a critical factor to adapt $Ls$. While different strategies including constant assigning and adaptation as a function of the velocity revealed an unacceptable behavior, the proposed fuzzy and continuous $Ls$ have manifested major robustness to sudden variation of road conditions. Scenario 2 elucidated the superior performance of the proposed approaches in path-tracking and the capability of reducing energy consumption in critical road situations. Scenario 3 confirmed the compromise between energy consumption and path-tracking of the fuzzy and continuous $Ls$ during daily driving. Finally, Scenario 4 showed the leading performance of the continuous $Ls$ over the fuzzy $Ls$ in terms of path-tracking, energy consumption, and vehicle stability.

A further advantage of employing the continuous $Ls$ over the fuzzy approach is its remarkable computational efficiency. The execution time of the look-ahead distance computation has been recorded in both the fuzzy and continuous approaches, where the simulations are conducted under an Intel Core i9-12950HX CPU 2.3-GHz laptop. Table 5 presents the recorded data in each scenario where the simulation time refers to the total time of the test, and the execution time of each approach is averaged by 10 runs. One can readily notice that the execution time to calculate the look-ahead distance based on the continuous function in the four scenarios is roughly 100 times faster than that based on the fuzzy logic approach. Therefore, the continuous $Ls$ operates in real-time without the need for dedicated computational hardware, unlike the fuzzy $Ls$, which relies on relatively high-performance computing hardware.

Videos of the validation on the SCANeR$^{TM}$ Studio simulator are given in a playlist at the following link "`https://www.youtube.com/playlist?list=PL6pn13pjrt-CCB0NPS0BtZazWWWyPXQl1`".

## 6. Conclusion

Although it is a virtual parameter of the lateral controller, the look-ahead distance is a key parameter that significantly affects the performance of the autonomous vehicle. Diving deep into the impact of this parameter, this paper inferred a set of rules to adapt the look-ahead distance to three factors. Then, an explicit mathematical model is developed for the look-ahead distance as a function of the considered factors. Further, another approach is proposed to adapt the look-ahead distance based on fuzzy logic control. The two approaches are contrasted with other methods and with each other to emphasize the leading merits of the proposed formula in terms of path-tracking performance, vehicle stability, computational efficiency, and energy consumption. As a future work, the authors will consider implementing the lateral controller with the proposed look-ahead distance formula on a real experimental vehicle in a testing platform.

## Acknowledgements

This work is carried out within the framework of the V3EA project "Electric, Energy Efficient, and Autonomous Vehicle" (2021-2025), funded by the Research National Agency (ANR) of the French government.

## Disclosure statement

No potential conflict of interest was reported by the authors.

## Funding

This work is funded by the French National Research Agency (ANR).

## References

[1] Peng H, Wang W, An Q, et al. Path tracking and direct yaw moment coordinated control based on robust mpc with the finite time horizon for autonomous independent-drive vehicles. IEEE Transactions on Vehicular Technology. 2020;69(6):6053–6066.

[2] Cao X, Xu T, Tian Y, et al. Gain-scheduling lpv synthesis $h_\infty$ robust lateral motion control for path following of autonomous vehicle via coordination of steering and braking. Vehicle System Dynamics. 2022;61(4):1–24.

[3] Li X, Xu N, Guo K, et al. An adaptive smc controller for evs with four iwms handling and stability enhancement based on a stability index. Vehicle System Dynamics. 2021; 59(10):1509–1532.

[4] He X, Liu Y, Lv C, et al. Emergency steering control of autonomous vehicle for collision avoidance and stabilisation. Vehicle System Dynamics. 2019;57(8):1163–1187.

[5] Liu C, Liu H, Han L, et al. Multi-level coordinated yaw stability control based on sliding mode predictive control for distributed drive electric vehicles under extreme conditions. IEEE Transactions on Vehicular Technology. 2023;72(1):280–296.
[6] Ahmadian N, Khosravi A, Sarhadi P. Driver assistant yaw stability control via integration of afs and dyc. Vehicle System Dynamics. 2022;60(5):1742–1762.
[7] Botes W, Botha TR, Els PS. Real-time lateral stability and steering characteristic control using non-linear model predictive control. Vehicle System Dynamics. 2022;61(4):1–23.
[8] Waqas M, Ioannou P. Automatic vehicle following under safety, comfort, and road geometry constraints. IEEE Transactions on Intelligent Vehicles. 2023;8(1):531–546.
[9] Zhou X, Wang Z, Shen H, et al. Robust adaptive path-tracking control of autonomous ground vehicles with considerations of steering system backlash. IEEE Transactions on Intelligent Vehicles. 2022;7(2):315–325.
[10] Chen G, Yao J, Hu H, et al. Design and experimental evaluation of an efficient mpc-based lateral motion controller considering path preview for autonomous vehicles. Control Engineering Practice. 2022;123:105164.
[11] Tian Y, Yao Q, Wang C, et al. Switched model predictive controller for path tracking of autonomous vehicle considering rollover stability. Vehicle System Dynamics. 2022; 60(12):4166–4185.
[12] Ollero A, García-Cerezo A, Martínez J. Fuzzy supervisory path tracking of mobile robots1. IFAC Proceedings Volumes. 1993;26(1):277–282. 1st IFAC International Workshop on Intelligent Autonomous Vehicles, Hampshire, UK, 18-21 April.
[13] Kang CM, Lee SH, Chung CC. A comparative study of lane keeping system: Dynamic and kinematic models with look-ahead distance. In: 2015 IEEE Intelligent Vehicles Symposium (IV); 2015. p. 1038–1043.
[14] Wang R, Li Y, Fan J, et al. A novel pure pursuit algorithm for autonomous vehicles based on salp swarm algorithm and velocity controller. IEEE Access. 2020;8:166525–166540.
[15] Atoui H, Milanés V, Sename O, et al. Real-time look-ahead distance optimization for smooth and robust steering control of autonomous vehicles. In: 2021 29th Mediterranean Conference on Control and Automation (MED); 2021. p. 924–929.
[16] Xu F, Shen T. Look-ahead prediction-based real-time optimal energy management for connected hevs. IEEE Transactions on Vehicular Technology. 2020;69(3):2537–2551.
[17] Cui Q, Ding R, Wei C, et al. Path-tracking and lateral stabilisation for autonomous vehicles by using the steering angle envelope. Vehicle System Dynamics. 2021;59(11):1672–1696.
[18] Zhang C, Hu J, Qiu J, et al. A novel fuzzy observer-based steering control approach for path tracking in autonomous vehicles. IEEE Transactions on Fuzzy Systems. 2019; 27(2):278–290.
[19] Goel A, Chauhan S. Adaptive look-ahead distance for pure pursuit controller with deep reinforcement learning techniques. New York, NY, USA. Association for Computing Machinery; 2022.
[20] Shan Y, Zheng B, Chen L, et al. A reinforcement learning-based adaptive path tracking approach for autonomous driving. IEEE Transactions on Vehicular Technology. 2020; 69(10):10581–10595.
[21] Kuwata Y, Teo J, Fiore G, et al. Real-time motion planning with applications to autonomous urban driving. IEEE Transactions on Control Systems Technology. 2009; 17(5):1105–1118.
[22] Tan HS, Huang J. Design of a high-performance automatic steering controller for bus revenue service based on how drivers steer. IEEE Transactions on Robotics. 2014;30(5):1137–1147.
[23] Lombard A, Buisson J, Abbas-Turki A, et al. Curvature-based geometric approach for the lateral control of autonomous cars. Journal of the Franklin Institute. 2020;357(14):9378–9398.
[24] Ahn Y, Shin S, Kim M, et al. Accurate path tracking by adjusting look-ahead point in pure pursuit method. International Journal of Automotive Technology. 2021;22:119–129.

[25] Shan Y, Yang W, Chen C, et al. Cf-pursuit: A pursuit method with a clothoid fitting and a fuzzy controller for autonomous vehicles. International Journal of Advanced Robotic Systems. 2015;12(9):134.
[26] Hasegawa K, Konaka E. Three look-ahead distance scheme for lateral control of vision-based vehicles. In: 2014 Proceedings of the SICE Annual Conference (SICE); 2014. p. 660–665.
[27] Chen L, Liu N, Shan Y, et al. A robust look-ahead distance tuning strategy for the geometric path tracking controllers. In: 2018 IEEE Intelligent Vehicles Symposium (IV); 2018. p. 262–267.
[28] Shao L, Jin C, Lex C, et al. Robust road friction estimation during vehicle steering. Vehicle System Dynamics. 2019;57(4):493–519.
[29] Rajamani R, Phanomchoeng G, Piyabongkarn D, et al. Algorithms for real-time estimation of individual wheel tire-road friction coefficients. IEEE/ASME Transactions on Mechatronics. 2012;17(6):1183–1195.
[30] Rajamani R. Vehicle dynamics and control. 2nd ed. Springer; 2012.
[31] Utkin V. On convergence time and disturbance rejection of super-twisting control. IEEE Transactions on Automatic Control. 2013;58(8):2013–2017.
[32] Chebly A, Talj R, Charara A. Coupled longitudinal/lateral controllers for autonomous vehicles navigation, with experimental validation. Control Engineering Practice. 2019; 88:79–96.
[33] Roselli F, Corno M, Savaresi SM, et al. H control with look-ahead for lane keeping in autonomous vehicles. In: 2017 IEEE Conference on Control Technology and Applications (CCTA); 2017. p. 2220–2225.
[34] Kato S, Tsugawa S, Tokuda K, et al. Vehicle control algorithms for cooperative driving with automated vehicles and intervehicle communications. IEEE Transactions on Intelligent Transportation Systems. 2002;3(3):155–161.
[35] Mamdani EH. Applications of fuzzy algorithms for control of a simple dynamic plant. Proceedings of the IEEE. 1974;.